

Analysis of Sub-Ice-Shelf Tides in the Weddell Sea Using SAR Interferometry

by Laurie Padman, Doug MacAyeal, and Eric Rignot

To be published in the Filchner-Ronne Ice Shelf Program Report No. 13, 1999.

Analysis of Sub-Ice-Shelf Tides in the Weddell Sea Using SAR Interferometry

Laurie Padman

*Earth & Space Research, 1910 Fairview Ave. E., Suite 102,
Seattle, WA 98102-3620, USA.*

Doug MacAyeal

*Department of Geophysical Sciences, University of Chicago 5734 S. Ellis Ave.,
Chicago, IL 60637, USA.*

Eric Rignot

*Jet Propulsion Laboratory, California Institute of Technology, MS 300-235,
4800 Oak Grove Drive, Pasadena, CA 91109, USA.*

Introduction

Tides near and under floating ice shelves can influence heat transport into the sub-ice-shelf cavity, mixing of the under-ice water column, and the calving and subsequent drift of tabular icebergs. It is extremely difficult to collect ocean data in these environments. Fortunately, synthetic aperture radar (SAR) can provide information on ocean height variability under the ice shelves. The procedure involves creating a “differential SAR interferogram” (“DSI”). A simple SAR interferogram is the difference between two SAR images, and can be analyzed to show a combination of the time-varying vertical motion due to tides and other ocean processes, and the lateral ice flow of the glacial sheet. Then, by differencing two SAR interferograms to give a DSI, and assuming that the lateral ice flow is time-independent, the remaining signal can be attributed to ocean-forced vertical motion of the ice sheet. For simplicity, for most of this paper we will refer to the ocean-forced motion as “tidal motion” or “tides”, however we will show later that other signals can be significant.

A DSI image is not a simple map of ocean tides, being a finite-second-difference of the ice vertical displacement. Depending on the satellite orbit parameters, the DSI can also exclude displacement signals due to specific tidal constituents. For example, for a 1.0-day image separation, the S_2 tide (with period 12.00 h) cannot be detected, since the tidal wave has exactly the same phase at each satellite pass. The K_1 tide (23.93 h) is also only poorly resolved. Nevertheless, with appropriate orbit parameters and a sufficient number of DSI images for the same region, it is theoretically possible to determine the amplitude and phase of all major tidal constituents.

With present limitations on DSI images available to us, just one DSI for each of the Ronne and the Filchner Ice Shelves in the southern Weddell Sea (**Figure 1**), we cannot map individual tidal constituents based only on SAR data. We can, however, use comparisons of the DSI images with synthesized tidal DSI fields based on numerical ocean tidal models to demonstrate that the DSI method can actually provide useful tidal and other ocean signals.

This report is a summary of a paper that we have submitted to the *Journal of Geophysical Research* [Rignot et al., 1999].

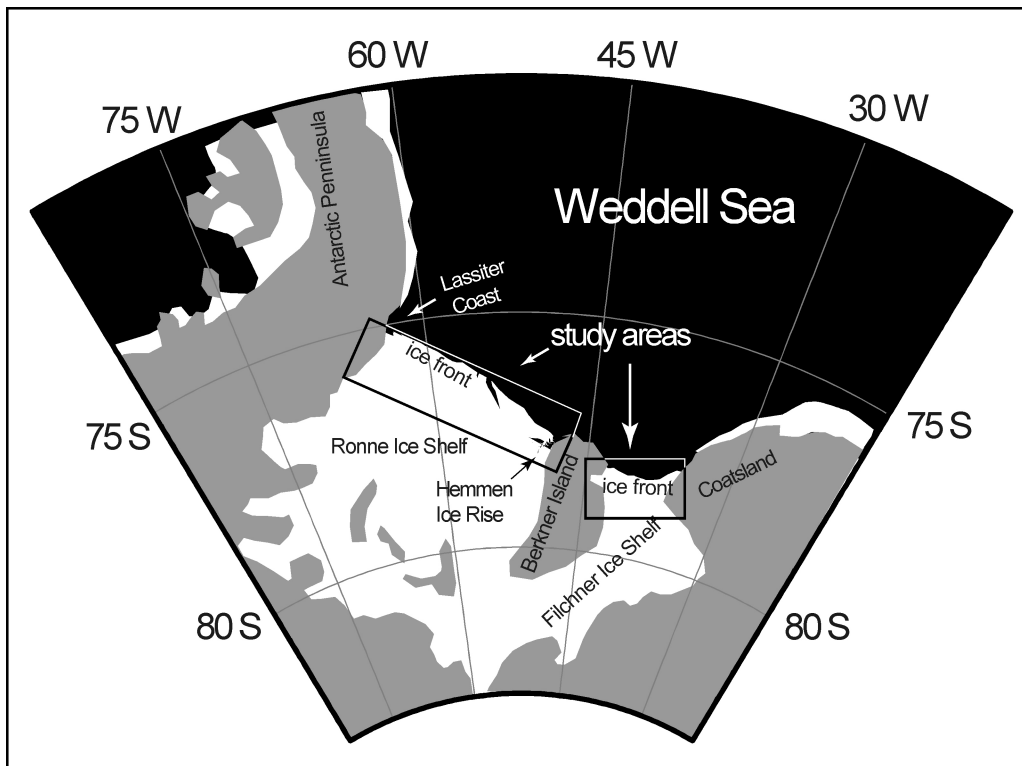


Figure 1: Map of the study region. The two rectangles denote the approximate areas covered by the differential SAR interferograms of the Ronne and Filchner Ice Shelf fronts. Gray areas are grounded ice, white areas are floating ice, and black is open water, including regions of perennial or seasonal sea ice.

SAR Processing

SAR data were provided by the European Space Agency (ESA) and were collected by the two Earth Remote Sensing satellites, ERS-1 and ERS-2. For the two regions studied (**Figure 1**), SAR data from 4 satellite passes, i.e., two pairs of passes, were used to construct DSI images. Following each pass of ERS-1 over a region of interest, ERS-2 passed over the same region almost exactly 1 day later. Each pair of satellite passes was separated by exactly 35 days, i.e., denoting the times of each pass as t_i , $i=1\dots 4$, then $(t_2-t_1)=(t_4-t_3)=24.00$ h, and $(t_3-t_1)=(t_4-t_2)=35.00$ days. For the Ronne Ice Shelf, the passes occurred on February 1 and 2, and March 7 and 8, 1996, each near 5:55 UTC. For the Filchner Ice Shelf, the passes occurred on January 15 and 16, and February 19 and 20, 1996, each near 6:28 UTC.

The raw information obtained from each SAR interferogram (difference between two SAR images) is the change in radar phase between the two images. This phase is “unwrapped” into radar range differences by integrating the phase from a region of no phase change (typically, grounded ice sheet or land) [Rignot and MacAyeal, 1998]. The resulting range displacement is then converted to vertical displacement using the radar illumination angle ($\approx 23^\circ$). Thus, each interferogram gives the difference in elevation between the two satellite passes. This signal, however, consists of a combination of vertical motion induced by the mean lateral flow of the ice sheet, and ocean-induced vertical motion. By assuming that the mean lateral flow is truly constant, subtracting one interferogram from another leaves only the ocean-induced vertical differential displacement, which we denote $\Delta\eta_{\text{DSI}}$.

Ocean Tidal Predictions

We use two ocean tidal models for comparison with the DSI images. One model is the global finite-element model denoted “FES95.2” [Le Provost *et al.*, 1998]. The other model is the Circum-Antarctic Tidal Simulation (“CATS99.2”), which is an extension of the Weddell/Scotia Sea tides model reported by *Robertson et al.* [1998]. CATS99.2 is a finite-element model of the World Ocean south of 50°S, and is solved on a 1/4° x 1/12° grid (about 10 km resolution along the Antarctic coast). Both models solve the depth-integrated shallow water equations with friction at the seabed and lateral viscosity providing sinks for tidal energy. FES95.2 has been tuned through formal assimilation of TOPEX/Poseidon satellite altimetry data (available only north of about 65°S because of satellite orbit geometry). CATS99.2 uses the FES95.2 model to provide open boundary conditions along 50°S.

The procedure for developing the synthetic DSI images from each tide model is as follows. First, tidal predictions are made for each of the four times, t_i , of the SAR images used in creating the DSI. Then, the differencing is carried out in exactly the same manner as for the DSI. Denoting an instantaneous model tide field as $h_m(x,y,t)$, the synthetic DSI field is

$$\Delta h_m(x,y) = (h_m(x,y,t_4) - h_m(x,y,t_3)) - (h_m(x,y,t_2) - h_m(x,y,t_1)) \quad (1)$$

Each model evaluates eight primary tidal constituents, three diurnal and five semidiurnal (see **Table 1**). Initially, we used a simple summation of these primary constituents for predicting $h_m(x,y,t_i)$ with CATS99.2. The prediction package provided with FES95.2, however, added several constituents that are estimated by inference from the primary modeled constituents. The addition of these extra terms greatly improves the model prediction skill, thus we recoded the CATS99.2 prediction algorithm to also include inferred constituents. The increase in prediction skill by this method was dramatic. This was initially surprising to us, since ocean data comparisons with CATS99.2 indicated very satisfactory agreement. However, the second-differencing of the tidal signal when constructing the synthetic DSI highlights small errors in the time series prediction. This study indicated to us that, even though most tide height variance is captured by the primary constituents, inclusion of the minor tides is critical to accurately representing the tidal contribution to the differential displacements in a DSI.

Table 1: Period (in hours) of the 8 primary tidal constituents used in both tidal models. The four constituents accounting for most tide height variance are O_1 , K_1 , M_2 , and S_2 (bold).

Constituent	Q_1	O_1	K_1	$2N_2$	N_2	M_2	S_2	K_2
Period (h)	26.87	25.82	23.93	12.91	12.66	12.42	12.00	11.97

Discussion

Having created the DSI differential displacement map ($\Delta\eta_{\text{DSI}}(x,y)$) and the equivalent model fields $\Delta h_m(x,y)$ (eq. 1), we compare these fields to determine the accuracy of the models. In **Figure 2** we show Δh_m for the two models and $\Delta\eta_{\text{DSI}}$ for the Ronne Ice Shelf. The large-scale fields are very similar in all three cases, however the DSI and FES95.2 both show a small-scale feature (“bump-and-dimple”) centered near 76.5°S, 56°W, that is absent in the CATS99.2 field. In **Figure 3** we show point-by-point comparisons between each model and $\Delta\eta_{\text{DSI}}$ for both ice shelves. For the Ronne Ice Shelf, FES95.2 predicts $\Delta\eta_{\text{DSI}}$ very well. CATS99.2 appears to overestimate $\Delta\eta_{\text{DSI}}$, and, as we saw in **Figure 2**, also fails to capture

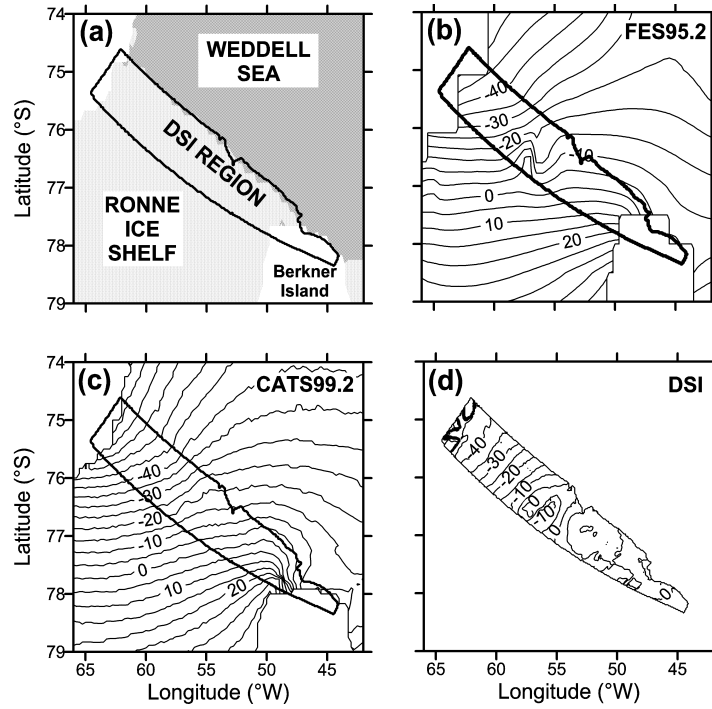


Figure 2: (a) outline of study area for Ronne Ice Shelf DSI. (b) FES95.2 predicted ocean tidal contribution to DSI ($\Delta h_{\text{FES95.2}}$). (c) CATS99.2 predicted ocean tidal contribution to DSI ($\Delta h_{\text{CATS99.2}}$). (d) Measured DSI differential displacement ($\Delta \eta_{\text{DSI}}$).

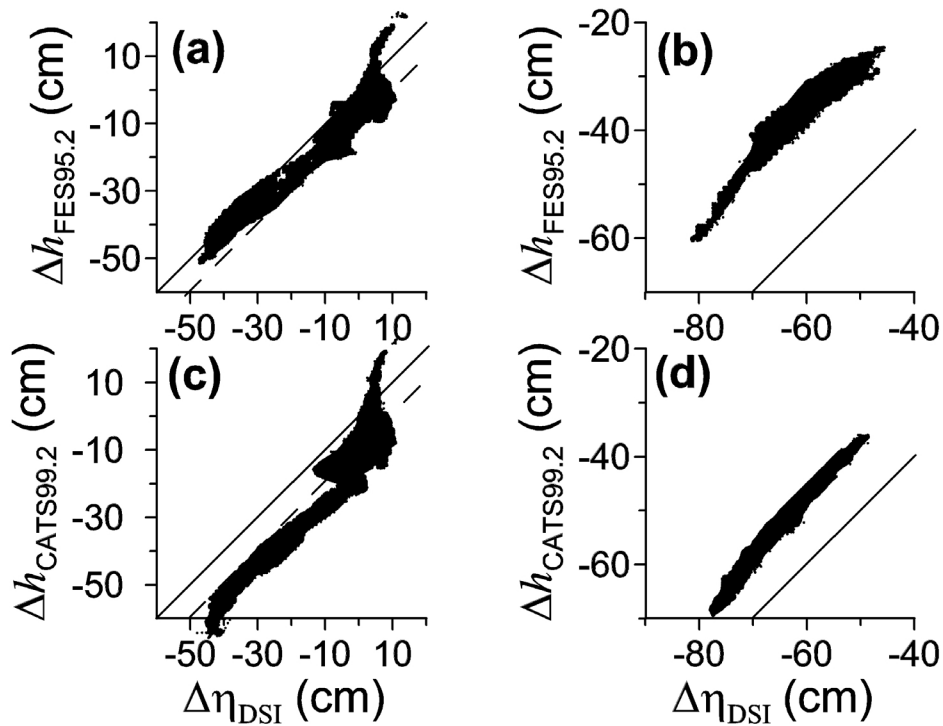


Figure 3: Comparison between ocean tidal model predictions, Δh_m , and the DSI observations, $\Delta \eta$. The top pair of panels is for FES95.2, and the bottom pair is for CATS99.2. Left panels refer to the Ronne Ice Shelf DSI, and right panels to the Filchner Ice Shelf DSI. Solid diagonal lines indicate model equivalence with data. Dashed lines in the left pair of panels indicate model equivalence when the inverse barometer effect of about 10 cm (see Table 2) is taken into account.

the bump-and-dimple feature. For the Filchner, FES95.2 overpredicts $\Delta\eta_{\text{DSI}}$ by about 20 cm, while CATS99.2 overpredicts $\Delta\eta_{\text{DSI}}$ by about 10 cm. In both cases, however, the error is large-scale, being almost constant over the entire image area. The error can be almost completely removed by small changes in the amplitude and/or phase of one of the dominant constituents, most likely O_1 or M_2 . The other major constituents, S_2 and K_1 , are excluded because their periods are too close to the satellite orbit separations.

We wanted to determine whether the differences between the modeled tides and the measured differential displacements of the ice shelves were due to model errors or to oceanographic processes that are not included in the ocean tidal models. One potentially significant non-tidal source of ocean height variability is the “inverse barometer effect” (“IBE”) [Gill, 1982, p. 337]. As atmospheric pressure (P_{atm}) decreases, the ocean surface responds by rising slightly. The IBE rate, assuming isostasy, is about 1 cm of ocean height increase for each 1 millibar (mb) increase of atmospheric pressure. Since 50 mb changes in P_{atm} are common at coastal stations around the Antarctic, ocean height can change by roughly 50 cm due to the IBE. The IBE contribution to the DSI is much smaller than this, however, because P_{atm} typically changes quite slowly, with time scales of several days. Thus, in a single interferogram based on two SAR images one day apart, the signal due to P_{atm} during this time is usually only a few cm. We used air pressure data recorded at Halley Base (75.5°S, 26.6°W: east of the Filchner Ice Shelf) and Butler Island (72.2°S, 60.3°W: west of the Ronne Ice Shelf) to investigate the expected contribution of the IBE to the two DSI images discussed in this paper. These values are presented in **Table 2**. Our analyses of the statistics for the IBE contribution to DSI images taken with the same set of relative times ($t_i - t_1$: $i=1 \dots 4$) but with arbitrary t_1 , shows that the standard deviation of the IBE contribution is about 9 cm, the mean value is close to zero (as expected), and maximum absolute values are about 20 cm. That is, errors of up to 20 cm in a comparison between a DSI synthesized from an ocean tide model and the measured DSI might be explained by the IBE.

From **Table 2**, and assuming that the tidal model is perfect and the IBE is isostatic, $\Delta\eta_{\text{DSI}}$ should exceed Δh_m by 9 cm for the Ronne image, while $\Delta\eta_{\text{DSI}}$ and Δh_m should agree for the Filchner image. The revised “equivalence” line for the Ronne Ice Shelf is shown as a dashed line on **Figure 3**. The fit between the CATS99.2 model and $\Delta\eta_{\text{DSI}}$ is much better when the IBE is included, so that this model’s inability to resolve the bump-and-dimple feature is its most serious defect. We conclude that the IBE is an identifiable signal in model comparisons with DSI images, and should be included in any attempts to explain ocean-forced vertical motion of the ice shelves.

Table 2: Inverse Barometer Effect (IBE) in cm, predicted for the Ronne and Filchner DSI images using surface air pressure recorded at 3-h intervals at Halley Bay and Butler Island. A positive value implies a positive contribution to the DSI. Halley Bay is the closest site to the Filchner Ice Shelf, while Butler Island is the closest site to the Ronne Ice Shelf.

Region	Butler Island	Halley Bay
Ronne Ice Shelf	+9	+12
Filchner Ice Shelf	+5	-1

Conclusions

Comparisons between ocean tidal models and SAR-derived vertical differential displacements of the Ronne and Filchner Ice Shelves show that:

- Tidal models for the southern Weddell Sea successfully predict the large-scale variability of ocean tidal loading on these ice shelves (away from grounding lines).
- The very high spatial resolution of the DSI (~40 m horizontal, and 1-2 mm in the vertical) shows significant tidal variability at small scales that are not well resolved by the models.
- The models are sufficiently accurate to allow us to demonstrate that non-tidal oceanic processes such as the IBE also influence the ice shelf vertical displacement.

The principal weaknesses in existing ocean tidal models for the southern Weddell Sea are due to the following problems:

1. poor bathymetry information, including water column thickness under the ice shelves;
2. the use of simplified friction parameterizations (benthic and under-ice drag coefficient and lateral viscosity) for removing tidal energy; and
3. inadequate grid resolution.

Except for weakness (3), above, these are difficult problems to solve, and a better approach to tidal modeling for ice shelves would be to use remote sensing data to directly map tides over the ice shelves in a manner analogous to the use of TOPEX/Poseidon satellite altimetry over the ice-free ocean surface. We show in *Rignot et al.* [1999] that, rather than simply using DSI data to validate models, we could instead use DSI data to directly map the spatial variability of tidal constituents under free-floating ice shelves. For this purpose, however, we would need many more independent DSI images for regions of interest to us than we presently have, and would also require different satellite orbit characteristics. The present, almost exactly one day separation of SAR images in individual interferograms prevents us from resolving the S_2 and K_1 tides, which are two of the four most energetic constituents (see **Table 1**).

Acknowledgments: Work at the Jet Propulsion Laboratory, California Institute of Technology was supported by a contract with the National Aeronautics and Space Administration (NASA). Support for the University of Chicago component of this project was provided by NASA (NAGW-5-4087) and the National Science Foundation Office of Polar Programs (OPP-9818622). The satellite data needed for this research were provided by the European Space Agency (ERS-1/2 project code: AO2.USA.160). The ocean tidal modeling at Oregon State University (OSU) and Earth & Space Research (ESR) was supported by grants from the National Science Foundation Office of Polar Programs (OPP-9615525 and OPP-9896041), and from NASA (NAG5-7790). We thank Charlie Werner for providing a SAR processor to generate the SAR interferograms, Andrew Gabriel for help in the project inception, and David Vaughan, Chris Doake, Richard Froelich, Richard Hindmarsh and other colleagues at the British Antarctic Survey for providing ice-thickness data for the FRIS and for their many suggestions during the course of the research reported here. Jonathan Bamber provided a digital topographic map of Antarctica. Landsat MSS data (georeferenced by the Institut für Angewandte Geodaesie (IfAG), Frankfurt am Main) proved to be invaluable in the verification and refinement of SAR data georeferencing, and were provided courtesy of H. Bennat and J. Sievers. Gary Egbert and Lana Erofeeva at OSU provided advice and computer resources for running the tidal model. Christian Le Provost provided the tidal prediction package for the FES95.2 tidal model, and Susan Howard at ESR was responsible for running this package for us. We thank Philippe Techine for providing details of the FES95.2 bathymetry for the southern Weddell Sea.

References

- Le Provost, C. F. Lyard, J. M. Molines, M. L. Genco and F. Rabilloud, A hydrodynamic ocean tide model improved by assimilating a satellite altimeter-derived data set, *J. Geophys. Res.*, *103*, 5513-5529, 1998.
- Rignot, E., L. Padman, D. R. MacAyeal, and M. Schmeltz, Analysis of sub-ice-shelf tides in the Weddell Sea using SAR interferometry, submitted to *J. Geophys. Res.*, 1999.
- Rignot, E., and D. R. MacAyeal, Ice-shelf dynamics near the front of the Filchner-Ronne Ice Shelf, Antarctica, revealed by SAR interferometry, *J. Glaciol.*, *44*, 405-418, 1998.
- Robertson, R. A., L. Padman, and G. D. Egbert, Tides in the Weddell Sea, In: *Ocean, Ice, and Atmosphere: Interactions at the Antarctic Continental Margin*, edited by S. S. Jacobs and R. F. Weiss, Antarctic Research Series, Volume 75, 341-369, 1998.